Mathematical Biosciences and Engineering

https://www.aimspress.com/journal/mbe

MBE, 23(7): 2208–2227.
DOI: 10.3934/mbe.2026080
Received: 13 April 2026
Revised: 26 May 2026
Accepted: 06 July 2026
Published: 17 July 2026

Research article

A spatial SIS point pattern model with movement

Eka Suci Pramana Sari[1], **Nanang Susyanto** [1,*], **Fajar Adi-Kusumo**[1], **Atina Husnaqilati**[1] **and Fugo Takasu**[2]

[1] Department of Mathematics, Universitas Gadjah Mada, Yogyakarta, Indonesia
[2] Department of Environmental Science, Nara Women's University, Nara, Japan

* **Correspondence:** Email: nanang_susyanto@ugm.ac.id.

Abstract: Spatial epidemic dynamics are strongly affected by local interactions and by the movement of individuals. This study develops a susceptible–infected–susceptible (SIS) model based on point pattern dynamics with individual movement. The model extends the spatial SIS point pattern framework of Hamada and Takasu by allowing susceptible and infected points to move in continuous space. Disease transmission is represented by a distance-dependent infection kernel, and Gaussian, step-function, and exponential kernels are compared. Heuristic singlet and pair-density equations are derived to describe how infection, recovery, birth, death, and movement affect the spatial distribution of susceptible and infected individuals. Numerical simulations are used to illustrate the effects of kernel shape, infection range, and movement on singlet densities, pair correlations, and the temporal evolution of point patterns. The results show how spatial movement and distance-dependent transmission jointly shape infection spread in a recurrent-infection framework.

Keywords: spatial transmission; point pattern dynamics; SIS model; individual movement; mathematical modeling

1. Introduction

Mathematical epidemiology provides a fundamental framework for understanding infectious disease dynamics within populations. Classical non-spatial models focus exclusively on population counts and often assume homogeneous mixing, thereby neglecting the explicit spatial locations of individuals. Although such models provide a useful starting point for theoretical analysis, they are often insufficient for capturing transmission processes that are driven by local interactions, spatial heterogeneity, and individual movement. Spatial structure and mobility have therefore become important themes in epidemic modeling, including spatial persistence of infections [1], metapopulation mobility models [2], and epidemic networks [3]. Related developments in stochastic epidemic dynamics and reinfection-

type models can also be found in [4, 5].

Spatial SIS models are relevant for infections where recovery does not provide durable immunity or in which recurrent susceptibility is a suitable population-level approximation. They have been studied in several spatial and mobile-population settings, including SIS patch models with movement [6], reaction–diffusion models for spatial risk and population movement [7], nonlocal dispersal models with convolution-type movement [8], mobile individuals in two-dimensional domains [9], metapopulation mobility models [10], and spatial models for sexually transmitted infections [11]. These studies show that movement and spatial contact structure can strongly affect persistence, invasion, and the distribution of infection. Nevertheless, many spatial SIS models represent space through patches, networks, or reaction–diffusion equations rather than through an explicit point pattern of individuals in continuous space.

Recent advances in spatial epidemiological modeling have used point pattern dynamics to represent individuals explicitly as points in space. Point-process and pair-approximation approaches provide a bridge between stochastic individual-level processes and population-level spatial dynamics [12–14]. In particular, Hamada and Takasu [15] developed an analytical framework for a spatial SIS point pattern model and studied the equilibrium distribution of infection under static point configurations. In their formulation, infection occurs through a distance-dependent kernel, and the spatial structure of susceptible and infected points is described through singlet and pair densities. However, in many populations, the locations of individuals change over time and movement can alter the pair structure through which infection is transmitted.

Motivated by this limitation, the present study extends the spatial SIS point pattern framework of Hamada and Takasu [15] by incorporating individual movement mechanisms based on the moment formulation of Dieckmann and Law [16]. This extension, particularly through the movement terms in the pair-density equations, provides a spatially explicit representation of transmission dynamics by accounting for both interaction distance and movement-induced redistribution of individuals. For example, convolution terms such as $(m_S * C_{SS})$ describe how the pair density of susceptible individuals changes when one or both individuals in a pair move.

The novelty of this study is twofold. First, we present a simulation analysis of stochastic SIS point-pattern dynamics with individual movement and birth–death processes. Second, we develop a heuristic derivation of singlet and pair dynamics, which provides insight into the mechanisms underlying the simulation results. The numerical experiments are designed to illustrate representative dynamical regimes of the proposed moving spatial SIS point-pattern model and to examine how infection range, kernel shape, and movement affect the resulting singlet densities and pair correlations. This approach aims to clarify how spatial structure, infection kernels, and movement jointly influence infection spread. The rest of the paper is structured as follows: Section 2 presents the formulation of the spatial SIS model. Section 3 details the parameter settings employed in this study and discusses the simulation results. Lastly, Section 4 concludes the study.

2. Materials and methods

We consider a spatial point-pattern population in which each individual has an explicit location and belongs to one of two epidemiological classes, susceptible (S) or infected (I). Susceptible individuals may acquire infection through spatial interaction with infected individuals, whereas infected

individuals may recover and re-enter the susceptible class. Each individual is modeled as a point in the two-dimensional domain $\Omega = [0, 1) \times [0, 1) \subseteq \mathbb{R}^2$. For $i = 1, 2, \ldots, n$, the position of the i-th point is denoted by $\mathbf{x}_i \in \Omega$, where n represents the total population size. Each point is assigned one of the two epidemiological states, and transitions between states occur stochastically in continuous time. Periodic boundary conditions are imposed on the spatial domain, so that boundary effects are avoided.

An individual in state S can be infected by an individual in state I at rate

$$\beta(|\xi|) = \beta_0 \, k(|\xi|). \tag{2.1}$$

Here, ξ denotes the displacement from an infected point to a susceptible point, and $|\xi|$ denotes the distance between the two points. Transmission is determined only by the distance $r = |\xi|$ and is assumed to occur isotropically; hence, the risk of transmission depends only on separation distance and not on direction. Furthermore, β_0 gives the total infection intensity, and $k(|\xi|)$ is the infection kernel, namely, the transmission function generated by infected individuals [17, 18]. The infection kernel is assumed to satisfy the normalization condition

$$\int_{\Omega} k(|\xi|) \, d\xi = 1.$$

Because the computational domain is treated as a torus, displacements are interpreted periodically. For kernels with short effective range relative to the domain size, this normalization agrees with the corresponding whole-plane normalization up to negligible boundary effects.

In spatial epidemic models, the infection kernel characterizes the range over which transmission is likely to occur. Following [15], we consider three kernel types, each parameterized by $\sigma_I > 0$, which controls the infection range around an infected individual. Specifically, we use

$$k_g(r) = \frac{1}{2\pi\sigma_I^2} \exp\left(-\frac{r^2}{2\sigma_I^2}\right), \tag{2.2}$$

$$k_s(r) = \begin{cases} \frac{1}{4\pi\sigma_I^2}, & r \le 2\sigma_I, \\ 0, & r > 2\sigma_I, \end{cases} \tag{2.3}$$

$$k_e(r) = \frac{1}{\pi\sigma_I^2} \exp\left(-\frac{\sqrt{2}}{\sigma_I} r\right). \tag{2.4}$$

These three kernels represent different spatial transmission patterns:

1) The Gaussian kernel (2.2) assumes that transmission is strongest near the infection source and decreases rapidly with distance. The parameter $\sigma_I > 0$ controls the effective infection radius.

2) The step-function kernel (2.3) assumes a constant infection rate up to the radius $2\sigma_I$ and zero transmission beyond that radius. Thus, transmission is uniform within a bounded neighborhood and zero outside it.

3) The exponential kernel (2.4) uses an infection rate that decreases exponentially with distance, thereby permitting transmission over longer distances than the Gaussian kernel.

Figure 1 illustrates the infection-spread profile produced by each kernel.

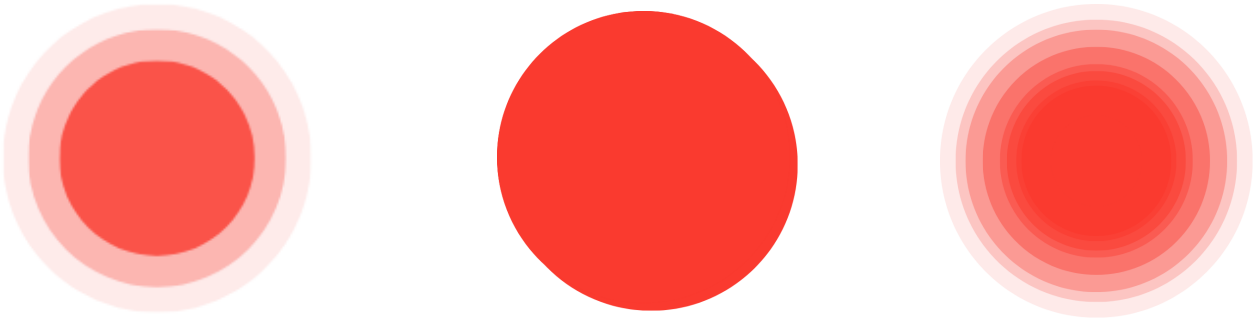

(a) Gaussian kernel **(b)** Step-function kernel **(c)** Exponential kernel

Figure 1. Illustration of the three transmission kernels.

To quantify the spatial range of transmission, the effective area of a kernel is given by

$$A = \left(\int_{\Omega} [k(r)]^2 \, d\xi \right)^{-1}.$$

Since three kernel types are considered, they are scaled so that all kernels share the same effective area [19]. Consequently, the effective area of each kernel in Eqs (2.2)–(2.4) is

$$A = \left(\frac{1}{4\pi\sigma_I^2} \right)^{-1} = 4\pi\sigma_I^2. \tag{2.5}$$

Taking both the kernel type and its effective area into account, the infection dynamics can be described as follows. An individual i in state S becomes infected with total rate $R_i(S \to I)$ given by

$$R_i(S \to I) = \sum_{\substack{j:\, x_j \in I \\ j \neq i}} \beta(|x_j - x_i|),$$

which represents the contribution of all infected points j with $j \neq i$, where $x_j - x_i$ is the vector from point i to point j.

Furthermore, an individual i in state I recovers to state S at a constant rate. That is,

$$R_i(I \to S) = \gamma.$$

The classical SIS dynamics without movement provide a basic representation of disease spread under a static point pattern. However, the assumption that point positions remain fixed over time may limit the model's ability to represent realistic epidemiological settings. Therefore, in the following subsection, the model is extended to incorporate point movement, allowing the spatial distribution and disease spread dynamics to be studied in a more detailed spatial framework.

2.1. SIS point pattern dynamics with movement

In the moving point-pattern model, the analysis is carried out at the level of individual points because movement changes locations continuously over time. Consequently, the spatial pattern of disease

spread can be represented more explicitly than in a static setting. In the model formulation, we make the following assumptions. Each susceptible and infected individual gives birth to a susceptible offspring at per-capita rate Λ. Susceptible individuals decrease through natural mortality at rate μS and become infected through interactions with infected individuals at rate $\beta S I$. The infected population decreases through natural mortality at rate μI and disease-induced mortality at rate δI. Infected individuals recover and return to the susceptible state at rate γI.

Table 1 summarizes the parameters used in the model.

Table 1. Model parameter notation.

Parameter	Description
Λ	Per-capita birth rate
β	Infection rate
δ	Disease-induced death rate
μ	Natural death rate
γ	Recovery rate
m	Movement rate
σ_I	Infection radius

The population-level SIS model is illustrated by the flow diagram in Figure 2.

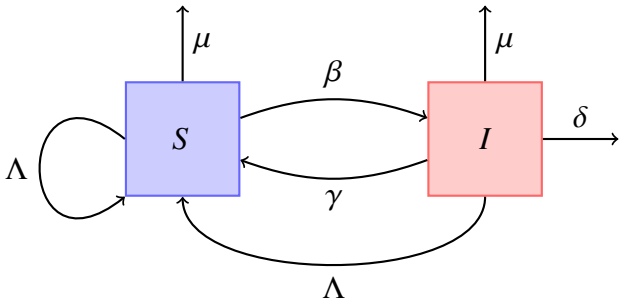

Figure 2. Flow diagram of the SIS transmission model with susceptible offspring produced at per-capita rate Λ by both susceptible and infected individuals.

Based on this flow diagram, we obtain the classical SIS model:

$$\begin{aligned} \frac{dS}{dt} &= \Lambda(S + I) - \beta S I + \gamma I - \mu S, \\ \frac{dI}{dt} &= \beta S I - (\gamma + \mu + \delta) I. \end{aligned} \tag{2.6}$$

Let N_S and N_I denote the singlet densities, that is, the numbers of individuals in states S and I per unit area. Furthermore, let $C_{SS}(\xi)$, $C_{SI}(\xi)$, $C_{IS}(\xi)$, and $C_{II}(\xi)$ denote the pair densities in status S–S, S–I, I–S, and I–I displaced by vector ξ, respectively. Motivated by the SIS model (2.6), we write the singlet dynamics as

$$\frac{d}{dt} N_S = \Lambda(N_S + N_I) - \int \beta(\xi) C_{SI}(\xi) d\xi + \gamma N_I - \mu N_S,$$

$$\frac{d}{dt}N_I = \int \beta(\xi)C_{SI}(\xi)d\xi - (\gamma + \mu + \delta)N_I,$$

where the birth term $\Lambda(N_S + N_I)$ reflects the assumption that offspring can be produced by either susceptible or infected parents and that all newborn individuals enter the susceptible state. The mean density, following [20], is given by

$$\langle N_S \rangle = \int S_x(x)\, dx, \quad \langle N_I \rangle = \int I_x(x)\, dx.$$

Here, A denotes the area of the spatial domain, and we set $A = 1$ without loss of generality. The spatial distributions of susceptible and infected individuals are represented by $S_x(x)$ and $I_x(x)$, respectively. An individual i at location $x_i = (x_{1_i}, x_{2_i})$ is represented by a Dirac delta function $\delta_{x_i}(x)$ centered at x_i. Therefore, the spatial distribution of individuals can be written as a sum of Dirac delta functions [19],

$$S_x(x) = \sum_{i=1}^{n} \delta(x - x_{i_S}) = \sum_{i=1}^{n} \delta_{x_{i_S}}(x),$$
$$I_x(x) = \sum_{i=1}^{n} \delta(x - x_{i_I}) = \sum_{i=1}^{n} \delta_{x_{i_I}}(x).$$

Using the Dirac delta function

$$\delta(x) = \begin{cases} \infty, & x = 0, \\ 0, & x \neq 0, \end{cases} \qquad \text{with the condition} \qquad \int_{-\infty}^{\infty} \delta(x)\, dx = 1,$$

we obtain

$$\langle N_S \rangle = \int \sum_{i=1}^{N_S} \delta_{x_i}(x)\, dx = \sum_{i=1}^{N_S} \int \delta_{x_i}(x)\, dx = \sum_{i=1}^{N_S} 1 = N_S,$$
$$\langle N_I \rangle = \int \sum_{i=1}^{N_I} \delta_{x_i}(x)\, dx = \sum_{i=1}^{N_I} \int \delta_{x_i}(x)\, dx = \sum_{i=1}^{N_I} 1 = N_I.$$

Accordingly, the dynamics of the mean singlet densities are

$$\begin{aligned} \frac{d}{dt}\langle N_S \rangle &= \frac{d}{dt}N_S \\ &= \Lambda(N_S + N_I) - \int \beta(\xi)C_{SI}(\xi)\, d\xi + \gamma N_I - \mu N_S \\ &= \Lambda(\langle N_S \rangle + \langle N_I \rangle) - \int \beta(\xi)\, C_{SI}(\xi)\, d\xi + \gamma\langle N_I \rangle - \mu\langle N_S \rangle, \end{aligned}$$

$$\begin{aligned} \frac{d}{dt}\langle N_I \rangle &= \frac{d}{dt}N_I \\ &= \int \beta(\xi)C_{SI}(\xi)\, d\xi - (\gamma + \mu + \delta)N_I \end{aligned}$$

$$= \int \beta(\xi) C_{SI}(\xi)\, d\xi - \gamma\langle N_I\rangle - \mu\langle N_I\rangle - \delta\langle N_I\rangle.$$

We define $|m_S| = \int m_S(\xi)\, d\xi$ and $|m_I| = \int m_I(\xi)\, d\xi$ as the total per capita movement rates of S and I, respectively, irrespective of direction [16]. In the simulations, the movement kernels are specified in Gaussian form as

$$m_S(\xi) = \frac{|m_S|}{2\pi\sigma_{mS}^2} \exp\left(-\frac{r^2}{2\sigma_{mS}^2}\right),$$
$$m_I(\xi) = \frac{|m_I|}{2\pi\sigma_{mI}^2} \exp\left(-\frac{r^2}{2\sigma_{mI}^2}\right),$$

where σ_{mS} and σ_{mI} control the displacement distances of S and I, respectively. At each birth event, the newborn susceptible individual is placed relative to the parent location according to the offspring-dispersal kernel $m_S^{(\Lambda)}(\xi)$. In the simulations, this kernel is specified as

$$m_S^{(\Lambda)}(\xi) = \frac{1}{2\pi\sigma_{bS}^2} \exp\left(-\frac{r^2}{2\sigma_{bS}^2}\right),$$

where σ_{bS} controls the spatial dispersal distance of a newly born susceptible individual. Furthermore, we define the Kronecker delta

$$\delta_{S,j} = \begin{cases} 1, & j = S, \\ 0, & j \neq S, \end{cases} \quad \text{and} \quad \delta_{I,j} = \begin{cases} 1, & j = I, \\ 0, & \text{otherwise.} \end{cases}$$

These indicators are used only to select the contributions associated with the relevant state in the birth and pair-formation terms.

2.2. Heuristic construction of the pair-density equations

The pair-density equations are assembled by tracking the events that create, destroy, or displace an ordered pair at separation ξ. Recovery and mortality give direct gain or loss terms because they change only the state of an individual in an existing pair. Infection terms are local in state but nonlocal in space: when an S individual in a pair is infected by a third I individual at displacement ξ', the rate depends on $\beta(\xi')$ and therefore involves triplet densities such as T_{SSI} and T_{SII}. Birth terms create parent–offspring pairs and also create new pairs between the offspring and the neighbors of the parent. Movement contributes two types of terms. First, a pair at displacement ξ is lost when either member moves, giving terms proportional to the total movement rates $|m_S|$ and $|m_I|$. Second, a pair at displacement ξ is gained when a previous pair at displacement $\xi + \xi'$ or $\xi - \xi'$ is shifted by a movement displacement ξ', giving convolution terms involving m_S or m_I. Thus, the movement kernels enter the pair equations through redistribution of pair separations rather than through changes in epidemiological state. The resulting system is exact only up to the unresolved triplet densities; the closure approximation introduced below is used to obtain a closed singlet–pair description. The pair-density dynamics are given by

$$\frac{d}{dt}C_{SS}(\xi) = \underbrace{2\delta_{SS}\Lambda m_S^{(\Lambda)}(-\xi)N_S}_{(1)} + \underbrace{\Lambda \int m_S^{(\Lambda)}(\xi')C_{SS}(\xi+\xi')\, d\xi'}_{(2)}$$

$$
\begin{aligned}
&+ \underbrace{\gamma C_{SI}(\xi) + \gamma C_{IS}(\xi)}_{(3)} \\
&- \underbrace{\int \beta(\xi') T_{SSI}(\xi, \xi')\, d\xi' - \int \beta(\xi') T_{SSI}(-\xi, \xi')\, d\xi'}_{(4)} \\
&- \underbrace{\mu C_{SS}(\xi) + \mu C_{SS}(\xi)}_{(5)} - \underbrace{2|m_S| C_{SS}(\xi)}_{(6)} \\
&+ \underbrace{\int m_S(-\xi') C_{SS}(\xi' + \xi)\, d\xi'}_{(7)} + \underbrace{\int m_S(-\xi') C_{SS}(\xi' - \xi)\, d\xi'}_{(8)},
\end{aligned} \tag{2.7}
$$

where m_S and m_I denote spatially homogeneous movement rates [16]. Thus, individual movement depends only on displacement and not on the absolute location x or the surrounding spatial configuration. The movement rate may differ between susceptible individuals (S) and infected individuals (I). The color coding used in the geometric illustrations is summarized in Table 2.

Table 2. Color interpretation.

Node Color	Interpretation
Susceptible (S)	An individual with susceptible state (S)
Birth	A newly born individual in state S
Recovery	An individual returning to state S through recovery
Movement	An individual undergoing movement
Infected (I)	An infected individual (I)
Death	The death of an individual (natural or disease-induced)
Infection	An individual becoming infected through contact with an infected neighbor

The terms in Eq (2.7) are interpreted in Table 3.

Table 3. Description of Eq (2.7).

Term	Equation	Description	Geometrical Illustration
1	$2\delta_{SS}\Lambda m_S^{(\Lambda)}(-\xi)N_S$	The $S-S$ pair density at distance ξ increases through the formation of new parent-offspring pairs after the birth of susceptible individuals. The factor δ_{SS} indicates that this contribution applies to $S-S$ pairs. The product ΛN_S gives the rate of birth events, while $m_S^{(\Lambda)}(-\xi)$ describes the spatial density of parents around their offspring at separation ξ.	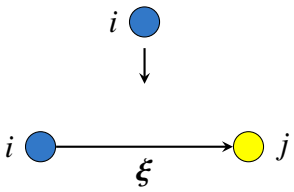
2	$\Lambda \int m_S^{(\Lambda)}(\xi')C_{SS}(\xi+\xi')\,d\xi'$	The second term also describes births, but now for newly formed pairs between the offspring and an S-neighbor of its parent. If an S individual belonging to an $S-S$ pair at distance $\xi+\xi'$ gives birth to a new individual at distance ξ' from the parent, then a new $S-S$ pair is created at distance ξ. Here, Λ is the birth rate, $C_{SS}(\xi+\xi')$ is the density of $S-S$ pairs at distance $\xi+\xi'$, and $m_S^{(\Lambda)}(\xi')$ is the spatial density of offspring around the susceptible parent.	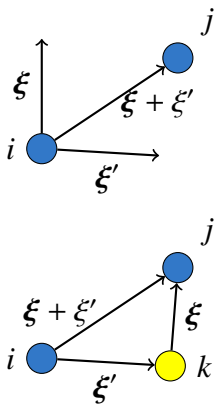

Continued on next page

Term	Equation	Description	Geometrical Illustration
3	$\gamma C_{SI}(\xi) + \gamma C_{IS}(\xi)$	The third term shows how recovery affects the density of $S-S$ pairs. In particular, when an infected individual in an $S-I$ or $I-S$ pair recovers to state S, that pair is converted into an $S-S$ pair.	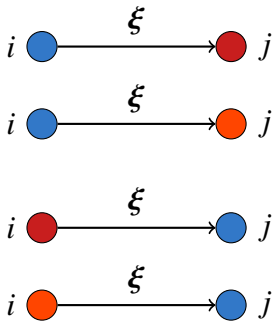
4	$\int \beta(\xi')T_{SSI}(\xi,\xi')\,d\xi' - \int \beta(\xi')T_{SSI}(-\xi,\xi')\,d\xi'$	The fourth term represents the loss of an $S-S$ pair when one of its members becomes infected through interaction with a third individual in state I.	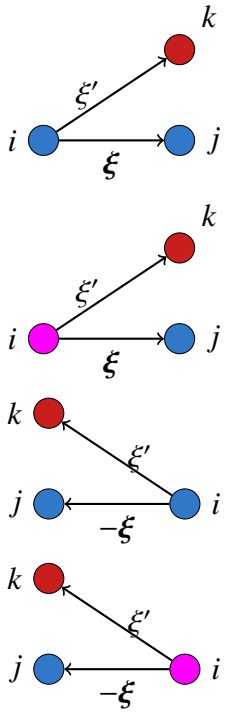

Continued on next page

Term	Equation	Description	Geometrical Illustration
5	$-\mu C_{SS}(\xi) - \mu C_{SS}(\xi)$	The fifth term represents the decrease in $S-S$ pair density caused by the natural death of either susceptible individual in the pair.	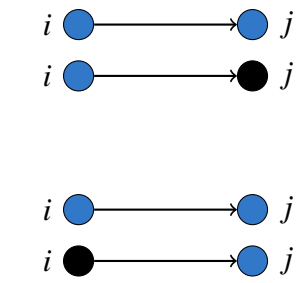
6	$2\lvert m_S\rvert C_{SS}(\xi)$	The sixth term describes the decrease in $S-S$ pair density when one of the susceptible individuals moves. Once either member of the pair changes position, the original pair at distance ξ is lost at per capita rate $\lvert m_S\rvert C_{SS}(\xi)$.	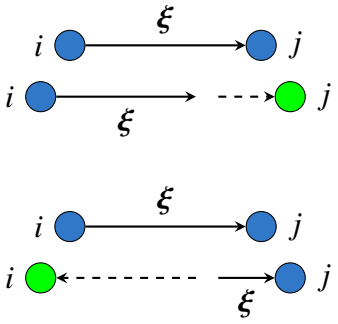
7	$\int m_S(-\xi')C_{SS}(\xi'+\xi)\,d\xi'$	The seventh term represents the increase in $S-S$ pair density caused by movement of susceptible individuals. A new pair with separation ξ is created when an individual from an initial pair with separation $\xi + \xi'$ moves by displacement ξ'.	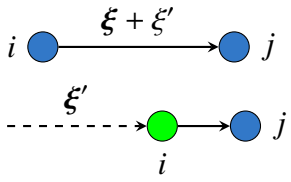
8	$\int m_S(-\xi')C_{SS}(\xi'-\xi)\,d\xi'$	The eighth term also describes the formation of new $S-S$ pairs through movement. In this case, a pair at distance ξ is generated from an initial separation $\xi' - \xi$ when a susceptible individual moves by $-\xi'$.	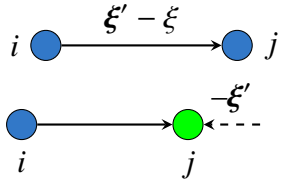

By symmetry, $C_{SI}(\xi) = C_{IS}(-\xi)$, meaning that the density of $S-I$ pairs with separation ξ is the same

as the density of $I-S$ pairs at the opposite displacement $-\xi$,

$$\begin{aligned}\frac{d}{dt}C_{SI}(\xi) &= \gamma\, C_{II}(\xi) - \gamma\, C_{SI}(\xi)\\ &\quad - \beta(\xi)\, C_{SI}(\xi) - \int \beta(\xi')\, T_{SII}(\xi,\xi')\, d\xi'\\ &\quad + \int \beta(\xi')\, T_{SSI}(-\xi,\xi')\, d\xi' + \Lambda\, m_S^{(\Lambda)}(-\xi)\, N_I\, \delta_{I,S}\\ &\quad + \Lambda \int m_S^{(\Lambda)}(\xi')\, C_{SI}(\xi+\xi')\, d\xi' \; - (\mu+\mu)\, C_{SI}(\xi)\\ &\quad - |m_S|\, C_{SI}(\xi) - |m_I|\, C_{SI}(\xi) + \int m_S(-\xi')\, C_{SI}(\xi+\xi')\, d\xi'\\ &\quad + \int m_I(-\xi')\, C_{IS}(\xi-\xi')\, d\xi' - \delta\, C_{SI}(\xi). \end{aligned} \tag{2.8}$$

Similarly, $C_{IS}(\xi) = C_{SI}(-\xi)$, which means that the density of $I-S$ pairs with separation ξ is the same as the density of $S-I$ pairs at the opposite distance $-\xi$,

$$\begin{aligned}\frac{d}{dt}C_{IS}(\xi) &= \gamma\, C_{II}(\xi) - \gamma\, C_{IS}(\xi)\\ &\quad - \beta(\xi)\, C_{IS}(\xi) - \int \beta(\xi')\, T_{SII}(-\xi,\xi')\, d\xi'\\ &\quad + \int \beta(\xi')\, T_{SSI}(\xi,\xi')\, d\xi' + \Lambda\, m_S^{(\Lambda)}(\xi)\, N_I\, \delta_{I,S}\\ &\quad + \Lambda \int m_S^{(\Lambda)}(\xi')\, C_{IS}(\xi-\xi')\, d\xi' \; - (\mu+\mu)\, C_{IS}(\xi)\\ &\quad - (|m_S| + |m_I|)\, C_{IS}(\xi) + \int m_I(-\xi')\, C_{IS}(\xi+\xi')\, d\xi'\\ &\quad + \int m_S(-\xi')\, C_{IS}(\xi-\xi')\, d\xi' - \delta\, C_{IS}(\xi). \end{aligned} \tag{2.9}$$

$$\begin{aligned}\frac{d}{dt}C_{II}(\xi) &= \beta(\xi)\, C_{SI}(\xi) + 2\int \beta(\xi')\, T_{SII}(\xi,\xi')\, d\xi'\\ &\quad - 2\gamma\, C_{II}(\xi) - 2\mu\, C_{II}(\xi) - 2|m_I|\, C_{II}(\xi)\\ &\quad + \int m_I(-\xi')\, C_{II}(\xi+\xi')\, d\xi' + \int m_I(-\xi')\, C_{II}(\xi-\xi')\, d\xi'\\ &\quad + 2\delta_{II}\Lambda m_I^{(\Lambda)}(-\xi) N_I + \Lambda \int m_I^{(\Lambda)}(\xi') C_{II}(\xi+\xi')\, d\xi'\\ &\quad - 2\delta\, C_{II}(\xi) + \beta(\xi)\, C_{IS}(\xi). \end{aligned} \tag{2.10}$$

Thus, the pair dynamics involve three triplet densities: (a) $T_{SSI}(\xi,\xi')$, the triplet density for the $S-S-I$ state with two displacement vectors ξ and ξ'; (b) $T_{SII}(\xi,\xi')$, the triplet density for the $S-I-I$ state; and (c) $T_{ISI}(\xi,\xi')$, the triplet density for the $I-S-I$ state. In this analysis, we assume the following

geometric symmetry:

$$\int \beta(\xi')T_{ISI}(\xi,\xi') = \int \beta(\xi')T_{SII}(\xi,\xi').$$

Consequently, the pair-density dynamics can be simplified by retaining the triplet densities $T_{SSI}(\xi,\xi')$ and $T_{SII}(\xi,\xi')$. We then approximate these triplet densities in terms of singlet and pair densities. The closure form is given by

$$T_{SSI}(\xi,\xi') = \frac{C_{SS}(\xi)\cdot C_{SI}(\xi')}{N_S}, \tag{2.11}$$

$$T_{SII}(\xi,\xi') = \frac{C_{SI}(\xi)\cdot C_{SI}(\xi')}{N_I}. \tag{2.12}$$

The closure approach used in this study is based on a symmetric pair approximation, in which third-order terms are approximated using first- and second-order information. This power-2 closure is adopted as a simple tractable closure that retains local spatial dependence through pair densities while avoiding a full hierarchy of triplet and higher-order densities. Its limitation is that genuine higher-order spatial correlations, including strong clustering or multi-point aggregation, are not represented explicitly. Therefore, the resulting model should be interpreted as a qualitative approximation to the full point-pattern dynamics rather than an exact description.

By substituting Eqs (2.11) and (2.12) into Eqs (2.7)–(2.10), one obtains a closed singlet-pair system. However, the resulting expressions contain multiple state labels, parent-offspring terms, and movement convolutions. Therefore, Eqs (2.7)–(2.10) together with the closure relations (2.11) and (2.12) are used as a heuristic closed approximation of the underlying point-pattern dynamics.

3. Point pattern dynamics simulation

Table 4 presents the numerical values of the model parameters used in the simulations. The parameter values are chosen to illustrate representative dynamical regimes of the moving spatial SIS point-pattern process and to compare the effects of infection range, kernel shape, and movement on the resulting dynamics.

Table 4. Baseline illustrative values used in the numerical simulations.

Notation	Simulation 1	Simulation 2	Unit	Role
$S(t=0)$	5000	80	individual	Initial susceptible population
$I(t=0)$	100	10	individual	Initial infected population
β_0	0.1	0.1	time^{-1}	Infection strength
γ	0.008	0.008	time^{-1}	Recovery rate
Λ	0.8	0.8	time^{-1}	Birth rate
δ	0.03	0.03	time^{-1}	Disease-induced death rate
μ	0.0002	0.0004	time^{-1}	Natural death rate
σ_I	0.01	0.02	distance scale	Infection range
$\lvert m_S\rvert$	7	7	time^{-1}	Total movement rate of susceptible individuals
$\lvert m_I\rvert$	7	7	time^{-1}	Total movement rate of infected individuals
σ_{mS}	0.01	0.01	distance scale	Movement range of susceptible individuals
σ_{mI}	0.01	0.01	distance scale	Movement range of infected individuals
σ_{bS}	0.01	0.01	distance scale	Offspring-dispersal range of newborn susceptible individuals

In the numerical simulations, the same total movement rate $|m_S| = |m_I| = 7$ is used for susceptible and infected individuals. The same spatial scale, $\sigma_{mS} = \sigma_{mI} = \sigma_{bS} = 0.01$, is used for susceptible movement, infected movement, and offspring dispersal. These values are treated as part of the illustrative simulation setup rather than as independently calibrated biological parameters. The time variable is therefore interpreted as a model time unit.

Figure 3 illustrates the infection-transmission pattern as a function of distance r for $\sigma_I = 0.01$. The Gaussian kernel attains high values at very short distances and then decreases sharply, indicating that transmission is concentrated locally and declines rapidly with distance. By contrast, the exponential kernel decreases more gradually, allowing transmission over longer distances, although with lower local intensity. The step-function kernel imposes a clear cutoff: it remains constant up to a distance of $r = 2\sigma_I$ and becomes zero beyond that point.

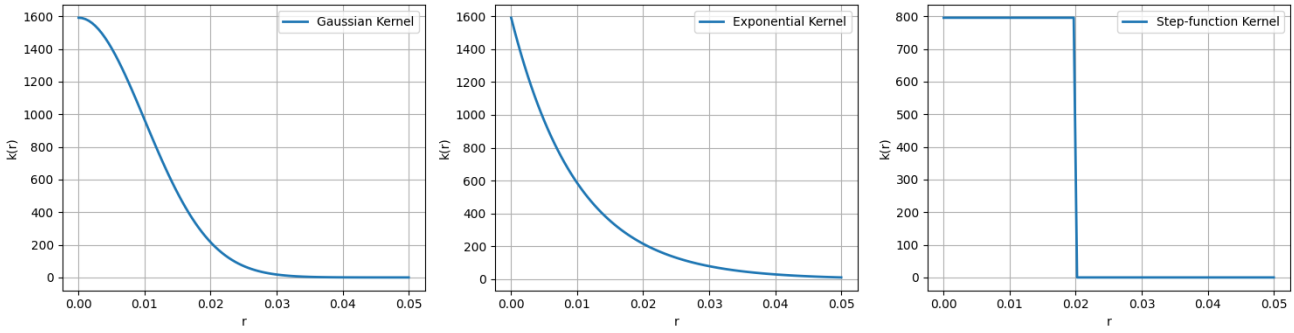

Figure 3. Infection kernels $k(r)$ for Gaussian, exponential, and step-function forms as a function of distance r with parameter $\sigma_I = 0.01$.

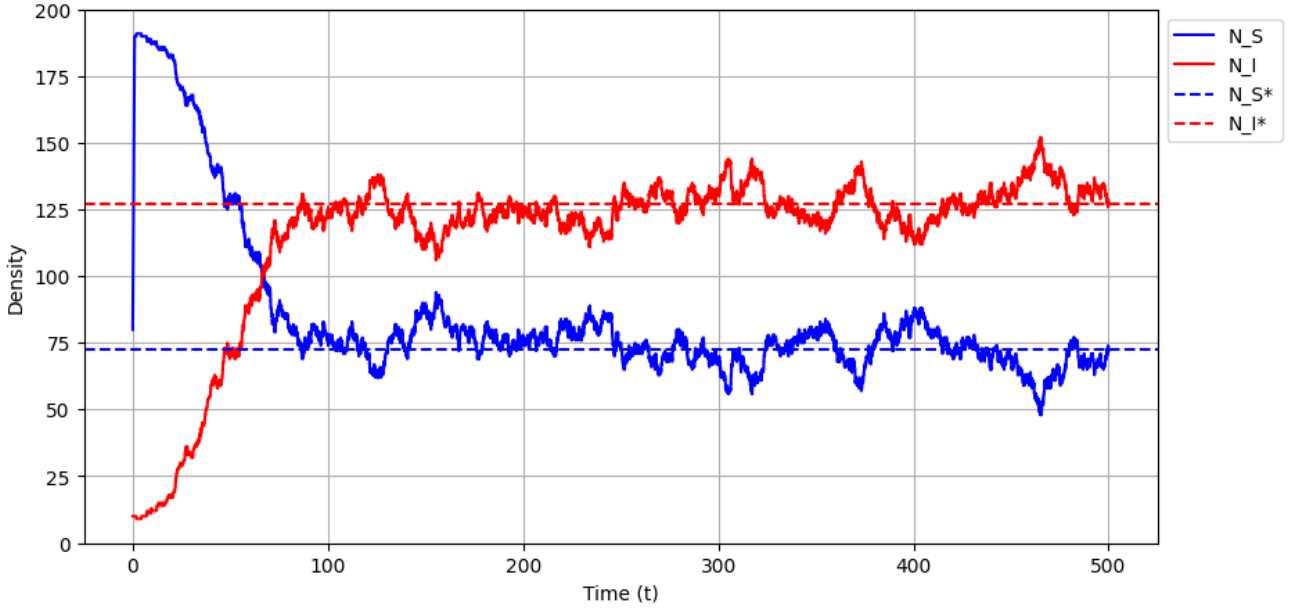

Figure 4. Singlet densities of susceptible and infected individuals.

Figure 4 shows the dynamics of the singlet densities. The simulation uses the parameter set given in

Simulation 2 of Table 4. At the beginning of the simulation, the density of infected individuals, $N_I(t)$, increases from its initial value and approaches approximately $N_I(500) \approx 128$. This increase occurs because the spatial infection rate, represented by the interaction integral $\int \beta(\xi) C_{SI}(\xi) d\xi$, initially exceeds the combined effects of recovery and mortality. In contrast, the density of susceptible individuals, $N_S(t)$, decreases during the early stage as susceptible individuals become infected.

The horizontal dashed lines denote numerically approximated steady-state values N_S^* and N_I^*, which are included only as reference levels for the long-term behavior of the singlet dynamics. At time $t = 500$, the density of susceptible individuals reaches $N_S(500) \approx 72$, whereas the density of infected individuals stabilizes at $N_I(500) \approx 128$. These results indicate that the system approaches an endemic regime in the illustrative parameter setting, with an infected density of about 128 per unit area and a susceptible density of about 72.

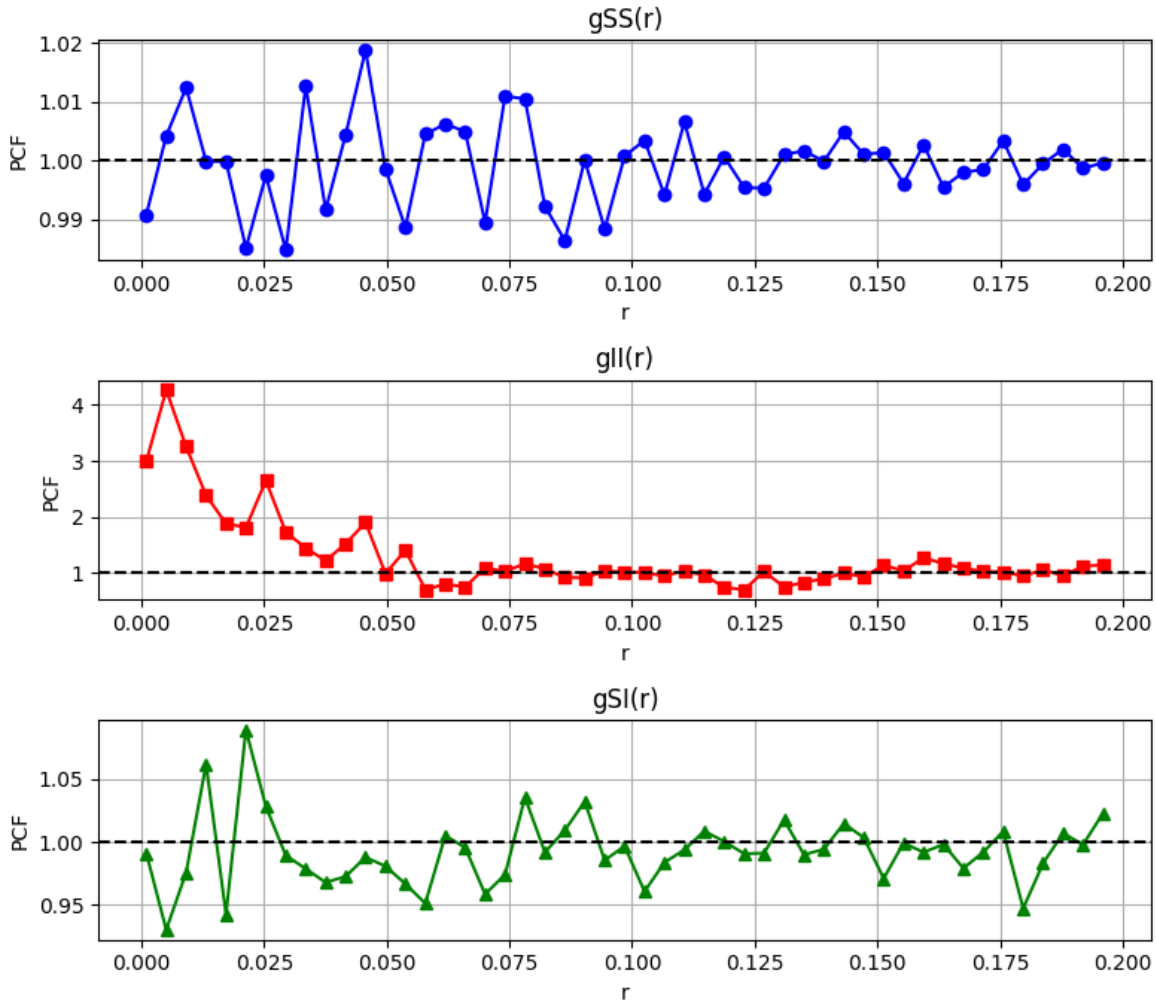

Figure 5. Pair correlation functions for susceptible-susceptible pairs $g_{SS}(r)$, infected-infected pairs $g_{II}(r)$, and susceptible-infected pairs $g_{SI}(r)$. The dashed lines indicate the reference level $g(r) = 1$ representing complete spatial randomness.

Figure 5 presents the pair correlation functions under complete spatial randomness (CSR) with the Gaussian kernel at the end of the simulation. The simulation uses the parameter set given in Simulation

1 of Table 4. These curves were obtained by normalizing pair counts with respect to the number of focal individuals, the annular area at distance r, and the corresponding singlet density, such that $g(r) = 1$ represents the reference level for a spatially uncorrelated configuration. In this figure, the curve of $g_{SS}(r)$ fluctuates narrowly around 1 across the entire range of r, indicating that susceptible–susceptible interactions are approximately consistent with random spatial mixing. Similarly, $g_{SI}(r)$ remains close to 1 with only slight local deviations, suggesting weak spatial association between susceptible and infected individuals. In contrast, $g_{II}(r)$ shows stronger fluctuations, particularly at small distances where values exceed 1, indicating a tendency for local clustering among infected individuals. This larger variability is expected due to the smaller number of infected individuals, which leads to noisier pair statistics. Overall, the figure highlights that while most spatial interactions are close to random, short-range clustering effects are more pronounced among infected individuals.

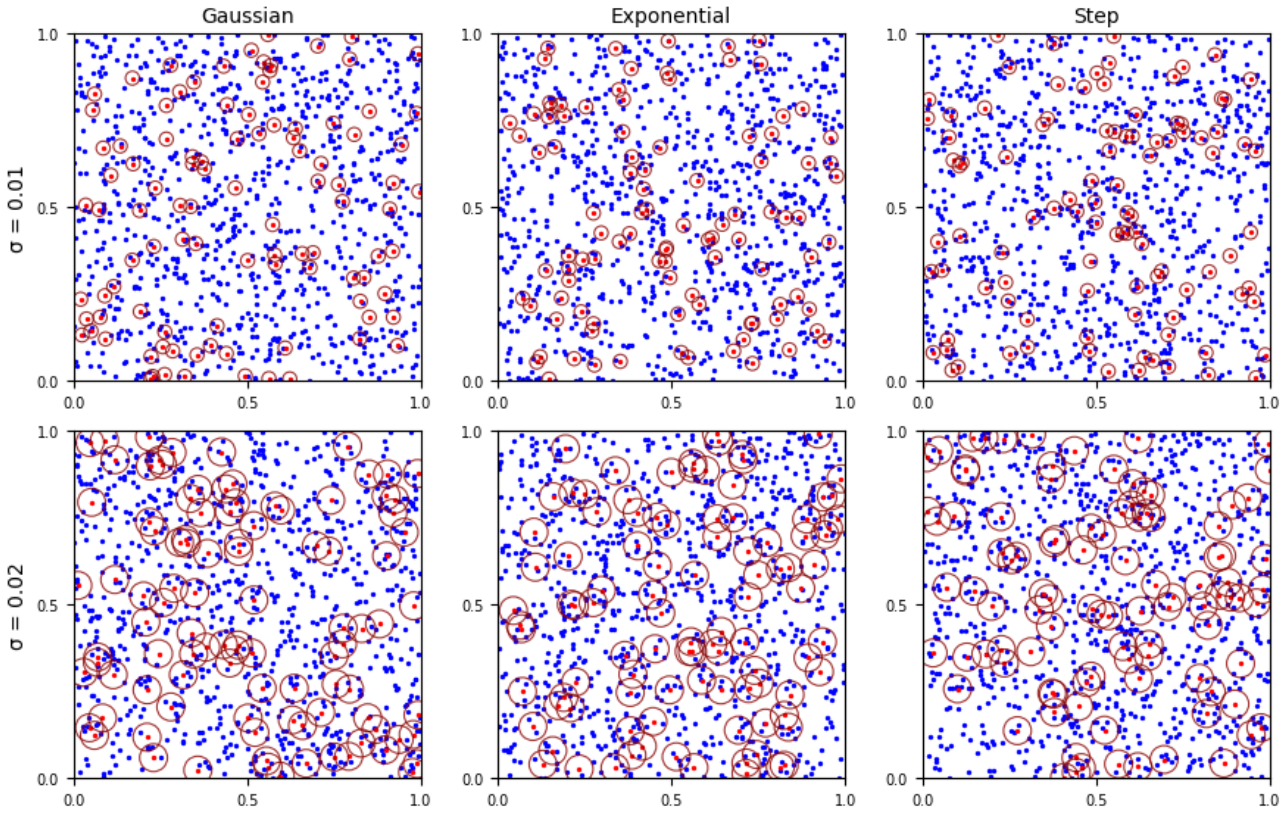

Figure 6. Point patterns for three kernels at $t = 0$.

Figure 6 illustrates the point pattern at $t = 0$. The initial conditions for susceptible and infected individuals are chosen to be comparable, producing identical point locations and an equal distribution of red and blue points across all three kernel types. The parameter $\sigma_I = 0.02$ represents a broader infection range than $\sigma_I = 0.01$. As σ_I increases, the infection range of each infected point expands, potentially facilitating faster disease spread within the spatial domain. Figure 7 then shows simulations of point patterns on CSR for two infection ranges, $\sigma_I = 0.01$ and 0.02, under the Gaussian, step-function, and exponential kernels.

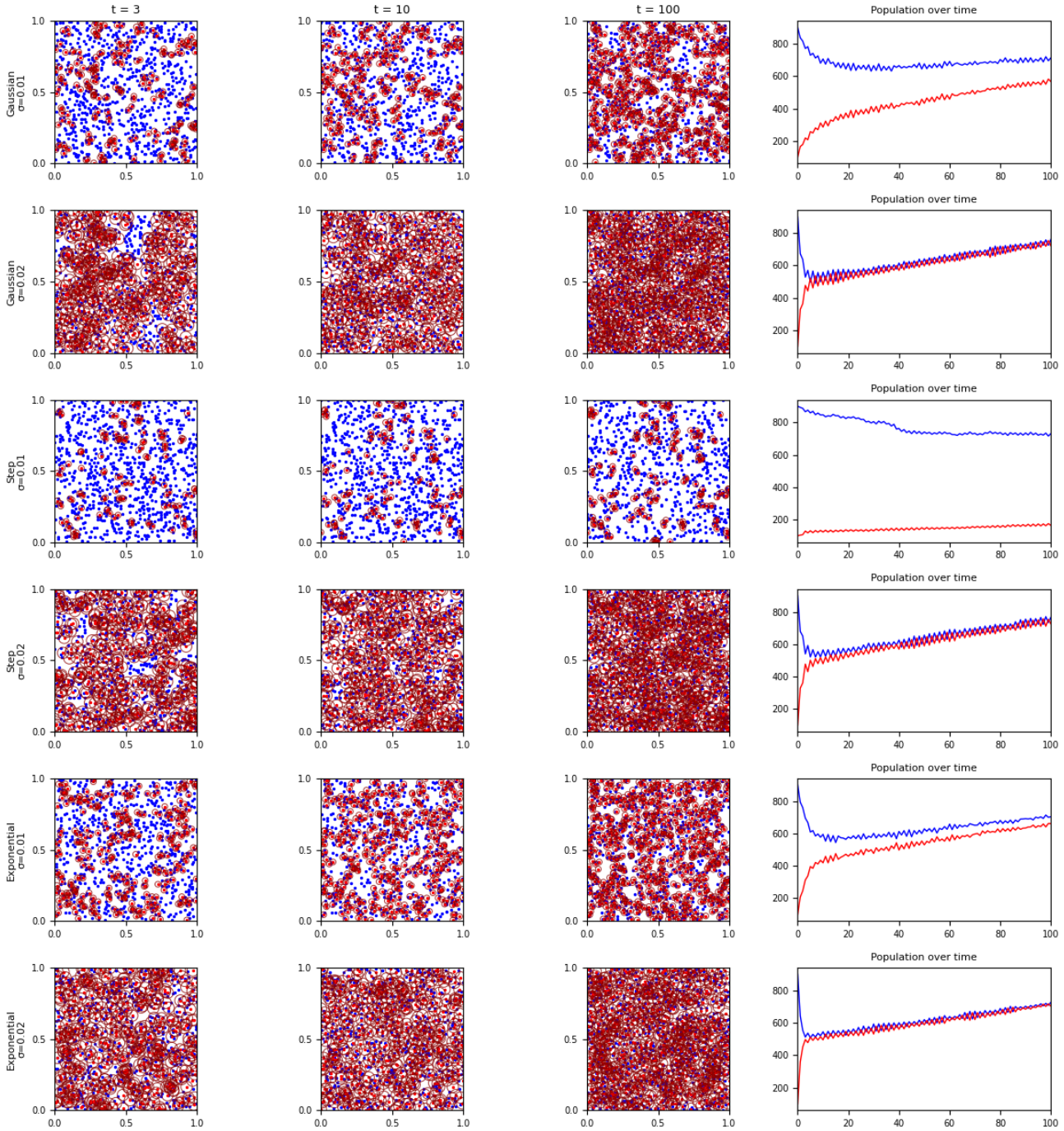

Figure 7. Temporal evolution of the point pattern on CSR for the three kernel types.

Figure 6 presents the point pattern at time $t = 0$, whereas Figure 7 shows the point patterns at times $t = 3, 10, 100$. For each kernel type, the number of infected points increases over time until the space is nearly completely occupied. When $\sigma_I = 0.02$, the space is filled more rapidly by infected points than when $\sigma_I = 0.01$, indicating that a larger infection range accelerates spatial transmission. The infection also propagates more rapidly under the exponential kernel than under the Gaussian and step-function kernels. This occurs because the exponential kernel decays more slowly with distance, so

infected individuals can still influence susceptible individuals located relatively far away. By contrast, the step-function kernel imposes a strict cutoff, which limits long-range transmission and leads to visibly slower spread. These point-pattern plots therefore illustrate the main effect of introducing spatial movement and distance-dependent transmission into the model: disease spread is governed not only by the numbers of susceptible and infected individuals, but also by how movement and kernel shape redistribute infection risk across space.

4. Conclusions

This study developed a moving spatial SIS model within the framework of point pattern dynamics. The model incorporates birth, death, and movement processes, thereby extending the static spatial SIS point pattern framework of Hamada and Takasu to a setting in which individual locations change over time. In this formulation, individuals are represented as points with explicit spatial locations and health states, namely, susceptible (S) or infected (I). By moving beyond classical non-spatial models, this approach captures local interactions and spatial heterogeneity through the use of several infection kernels (Gaussian, step-function, and exponential). We also derived heuristic moment dynamics for singlet and pair densities, supported by geometric interpretations of the pair-density terms.

The transition from S to I is governed by an infection rate with a distance-dependent kernel. The kernel type influences the form of this infection rate. For all three kernel types considered, the infection rate decreases as distance increases. In other words, the probability of infection declines as the spatial separation between susceptible and infected individuals becomes larger.

The numerical simulations show that the singlet density of infected individuals initially increases, while the singlet density of susceptible individuals decreases. In addition, the infection radius σ_I strongly affects the speed of spatial disease spread. The point-pattern snapshots suggest that σ_I also influences the spatial extent of infection. For $\sigma_I = 0.01$, the infection remains relatively localized, whereas for $\sigma_I = 0.02$, it expands more broadly in space. Thus, a larger infection radius σ_I leads to faster spatial expansion of the disease. This behavior is observed consistently across all kernel types and spatial point distributions. The results further indicate that the shape of the infection kernel influences spatial spread: the exponential kernel produces faster spread because it preserves non-negligible transmission over longer distances, whereas the step-function kernel spreads more slowly because of its finite cutoff. These findings indicate that spatial interaction characteristics play an important role in epidemic dynamics and reveal effects that non-spatial models cannot capture.

However, the model has certain limitations. The transmission mechanism relies solely on spatial distance and does not yet incorporate environmental heterogeneity, behavioral heterogeneity, or contact processes beyond the distance-dependent kernel. The movement model employed is also relatively basic: movement is isotropic, spatially homogeneous, and independent of local clustering. In addition, the singlet and pair-density dynamics are derived heuristically rather than rigorously from the full moment framework of Dieckmann and Law [16]. Furthermore, the model parameters have not been calibrated with empirical data.

Consequently, future research could focus on integrating empirical spatial data for parameter calibration, deriving the singlet and pair-density dynamics rigorously according to Dieckmann and Law [16], and enhancing the movement mechanism to include clustered, directed, or environment-dependent movement. Another important direction is to analyze the threshold and equilibrium structure

of the closed moment system. In stochastic point-pattern dynamics, however, a reproduction number or invasion criterion must account for the local spatial configuration around the initially infected individual, because infection may either spread or die out depending on the nearby susceptible neighborhood. A systematic study of reproduction numbers and invasion criteria for moving point-pattern epidemic dynamics is therefore reserved for future work.

Use of AI tools declaration

The authors declare that Artificial Intelligence (AI) tools were used only for language editing and improvement of grammar, clarity, and readability. The AI tools were not used to generate scientific content, develop the mathematical model, perform the analysis, or draw the conclusions. The authors take full responsibility for the content of this article.

Acknowledgments

This research was supported by the Ministry of Higher Education, Science, and Technology of the Republic of Indonesia under the Fundamental Research Scheme, grant numbers 067/C3/DT.05.00/PL/2025 and 2485/UN1/DITLIT/Dit-Lit/PT.01.03/2025.

Conflict of interest

The authors declare there is no conflict of interest.

References

1. B. M. Bolker, B. T. Grenfell, Space, persistence and dynamics of measles epidemics, *Phil. Trans. R. Soc. B*, **348** (1995), 309–320. https://doi.org/10.1098/rstb.1995.0070
2. D. Balcan, B. Gonçalves, H. Hu, J. J. Ramasco, V. Colizza, A. Vespignani, Modeling the spatial spread of infectious diseases: The global epidemic and mobility computational model, *J. Comput. Sci.*, **1** (2010), 132–145. https://doi.org/10.1016/j.jocs.2010.07.002
3. M. J. Keeling, K. T. D. Eames, Networks and epidemic models, *J. R. Soc. Interface*, **2** (2005), 295–307. https://doi.org/10.1098/rsif.2005.0051
4. D. Lestari, N. Y. Megawati, N. Susyanto, F. Adi-Kusumo, Qualitative behaviour of a stochastic hepatitis C epidemic model in cellular level, *Math. Biosci. Eng.*, **19** (2022), 1515–1535. https://doi.org/10.3934/mbe.2022070
5. N. Susyanto, Investigating the ARSIRI model: An extended SIR model with reinfection for modelling addiction-related phenomena, *Malaysian J. Math. Sci.*, **19** (2025), 311–323. https://doi.org/10.47836/mjms.19.1.16
6. L. J. S. Allen, B. M. Bolker, Y. Lou, A. L. Nevai, Asymptotic profiles of the steady states for an SIS epidemic patch model, *SIAM J. Appl. Math.*, **67** (2007), 1283–1309. https://doi.org/10.1137/060672522

7. R. Peng, F. Yi, Asymptotic profile of the positive steady state for an SIS epidemic reaction–diffusion model: Effects of epidemic risk and population movement, *Physica D*, **259** (2013), 8–25. https://doi.org/10.1016/j.physd.2013.05.006
8. F. Yang, W. Li, S. Ruan, Dynamics of a nonlocal dispersal SIS epidemic model with Neumann boundary conditions, *J. Differ. Equations*, **267** (2019), 2011–2051. https://doi.org/10.1016/j.jde.2019.03.001
9. Q. Pan, R. Liu, M. He, An epidemic model based on individuals with movement characteristics, *Physica A*, **399** (2014), 157–162. https://doi.org/10.1016/j.physa.2013.12.043
10. L. Meng, N. Masuda, Epidemic dynamics on metapopulation networks with node2vec mobility, *J. Theor. Biol.*, **534** (2022), 110960. https://doi.org/10.1016/j.jtbi.2021.110960
11. C. Castillo-Chavez, B. Li, Spatial spread of sexually transmitted diseases within susceptible populations at demographic steady state, *Math. Biosci. Eng.*, **5** (2008), 713–727. https://doi.org/10.3934/mbe.2008.5.713
12. C. T. Bauch, A. P. Galvani, Using network models to approximate spatial point-process models, *Math. Biosci.*, **184** (2003), 101–114. https://doi.org/10.1016/S0025-5564(03)00042-7
13. M. J. Keeling, D. A. Rand, A. J. Morris, Correlation models for childhood epidemics, *Proc. R. Soc. B*, **264** (1997), 1149–1156. https://doi.org/10.1098/rspb.1997.0159
14. M. J. Keeling, The effects of local spatial structure on epidemiological invasions, *Proc. R. Soc. B*, **266** (1999), 859–867. https://doi.org/10.1098/rspb.1999.0716
15. M. Hamada, F. Takasu, Equilibrium properties of the spatial SIS model as a point pattern dynamics - how is infection distributed over space, *J. Theor. Biol.*, **468** (2019), 12–26. https://doi.org/10.1016/j.jtbi.2019.02.005
16. U. Dieckmann, R. Law, Relaxation projections and the method of moments, in *The Geometry of Ecological Interactions: Simplifying Spatial Complexity*, (eds. U. Dieckmann, R. Law and J. A. J. Metz), Cambridge University Press, Cambridge, (2000), 412–455.
17. J. Dushoff, S. W. Park, Speed and strength of an epidemic intervention, *Proc. R. Soc. B*, **288** (2021), 20201556. https://doi.org/10.1098/rspb.2020.1556
18. D. Mollison, Dependence of epidemic and population velocities on basic parameters, *Math. Biosci.*, **107** (1991), 255–287. https://doi.org/10.1016/0025-5564(91)90009-8
19. B. M. Bolker, Analytic models for the patchy spread of plant disease, *Bull. Math. Biol.*, **61** (1999), 849–874. https://doi.org/10.1006/bulm.1999.0115
20. D. J. Murrell, U. Dieckmann, R. Law, On moment closures for population dynamics in continuous space, *J. Theor. Biol.*, **229** (2004), 421–432. https://doi.org/10.1016/j.jtbi.2004.04.013

AIMS Press